RSC Advances

PAPER

View Article Online
View Journal | View Issue

Cite this: *RSC Adv.*, 2025, **15**, 12528

Efficient separation of Mg^{2+}/Li^{+} using reduced GO membranes modified by positively charged arginine†

Junbo Wang,‡[a] Jie Jiang,‡[a] Jing Wang,[a] Shouyuan Hu,[a] Jiahao Hu,[a] Yalong Li,[a] Zhiyu Tao,[a] Chengju Wu,[a] Pei Li *[ab] and Liang Chen [a]

Nanofiltration has emerged as an effective technique for the selective separation of mono- and divalent ions, such as Mg^{2+}/Li^{+} mixtures, and plays a crucial role in lithium extraction from salt lakes. In this study, a graphene oxide (GO) membrane with positively charged channels was prepared by crosslinking arginine (Arg) onto GO nanosheets, followed by vacuum filtration to form the membrane, and then thermal reduction (Arg-rGO). The Arg-rGO membrane exhibits high performance in the ion separation of a typical brine with a Mg^{2+}/Li^{+} mass ratio of 20. The separation factor ($S_{Li/Mg}$) reached up to 45.6—two times the highest separation factor reported—while maintaining an advanced water permeance of 21.3 L m^{-2} h^{-1} bar^{-1}. Furthermore, the Mg^{2+}/Li^{+} mass ratio was reduced from 20 to 0.2 after two-stage crossflow filtration with high flux under high pressure. The observed separation performance can be attributed to the synergistic effect of electrostatic repulsion and size-exclusion. These findings confirmed efficient separation of Mg^{2+}/Li^{+} using GO membranes, demonstrating potential for practical application in lithium extraction from salt lakes.

Received 24th January 2025
Accepted 10th April 2025

DOI: 10.1039/d5ra00580a

rsc.li/rsc-advances

1. Introduction

The rapid expansion of lithium-based energy sources has significantly increased global demand for lithium, leading to a severe shortage of this critical resource.[1–3] Lithium is primarily extracted from lithium-bearing minerals and lithium-containing water,[4,5] and brines account for over 60% of current production.[6] However, the extraction of lithium from salt lake brines or seawater presents significant challenges due to the presence of numerous other ions with similar sizes and properties,[7] such as K^{+}, Na^{+}, Ca^{2+}, and Mg^{2+}. In particular, the separation of Mg^{2+} and Li^{+} ions is a challenging process, primarily due to their nearly identical sizes and the high Mg^{2+}/Li^{+} mass ratio.[8] Various strategies have made advancements in lithium extraction, including precipitation,[9,10] extraction,[3,11] and adsorption;[12,13] however, these strategies are still hindered by high energy consumption, low efficiency, and environmental concerns.[14–16]

Membrane technologies, especially two-dimensional (2D) membranes, have been considered as potentially efficient methods for extracting Li^{+} from brine or seawater, owing to their ability to precisely control sub-nanometer interlayer spacing[17,18] and convenient interfacial functionalization,[19,20] as well as their low energy consumption and environmental sustainability.[21,22]

Graphene oxide (GO), a representative 2D material with negatively charged functional groups, has been extensively explored for molecular and ion sieving applications.[23–26] Crosslinking or charge modification represents a promising approach to enhance the ion separation performance of GO-based membranes.[27,28] These approaches generally involve self-assembly[29,30] and surface coating[31,32] to modify GO membrane with charged long-chain polymers,[33,34] resulting in the distortion and expansion of the interlayer spacing.[33,35,36] Obviously, an increase in interlayer spacing reduces the effectiveness of membranes in achieving electrostatic repulsion and precise size exclusion of salt ions of minimal size. For example, crosslinking with polyethyleneimine (PEI) resulted in positively charged GO membranes that exhibited a moderate separation factor of 5.7 in the ion separation of Mg^{2+}/Li^{+}, with a rejection rate of 85.3% for Mg^{2+} and a rejection rate of 16.7% for Li^{+} during the separation of a Mg^{2+}/Li^{+} brine.[37] Therefore, further research on charge modification and interlayer spacing control of GO-based membranes is necessary to enhance their performance in lithium extraction from salt lakes.

In this study, we have fabricated a GO membrane that incorporates positively charged GO nanosheets, which have been modified with Arg amino acid and subsequently undergo

[a]School of Physical Science and Technology, Ningbo University, Ningbo 315211, China. E-mail: lipei@nbu.edu.cn
[b]State Key Laboratory of Surface Physics and Department of Physics, Fudan University, Shanghai 200433, China

† Electronic supplementary information (ESI) available. See DOI: https://doi.org/10.1039/d5ra00580a

‡ These authors contributed equally.

thermal reduction (Arg-rGO). The Arg-rGO membrane has positively charged nanochannels and controlled interlayer spacing, which provides stability that effectively inhibits the swelling of the nanosheets in aqueous solutions. Importantly, the Arg-rGO membrane exhibits high performance in the ion separation of Mg^{2+}/Li^{+} with $S_{Li/Mg}$ of 45.6, while maintaining an advanced water permeance of 21.3 L m^{-2} h^{-1} bar^{-1}. By a two-step high-pressure crossflow at a pressure of 3 bars, the Arg-rGO membrane achieves a Mg^{2+}/Li^{+} mass ratio of 0.2 with high flux from a typical brine with a mass ratio of 20. Additionally, the membrane displays exceptional performance when subjected to various parameters, including ion types, ratios, concentrations, and pH values.

2. Experimental section

2.1. Chemicals

Graphite powder (8000 mesh, 99%), arginine (Arg, 99%), sulfuric acid (H_2SO_4), hydrochloric acid (HCl), phosphorus pentoxide (P_2O_5), potassium permanganate ($KMnO_4$), 1-(3-dimethylaminopropyl)-3-ethylcarbodiimide (EDC, 97%), *N*-hydroxysuccinimide sodium salt (NHS, 98%), sodium hydroxide (NaOH), anhydrous lithium chloride (LiCl), and anhydrous magnesium chloride ($MgCl_2$) were purchased from Aladdin's reagent (Shanghai). Additionally, dialysis bags with a molecular weight cut-off (MWCO) of 12–14 kDa were sourced from Hunan Bikman Biotechnology. MCE membranes with a pore size of 0.22 μm were provided by Tianjin Jinteng Experimental Equipment Co., Ltd.

2.2. Preparation of Arg-GO nanosheets

Graphene oxide (GO) nanosheets were initially synthesized using a modified Hummers' method (specific steps in the ESI†). Subsequently, 100 mg of the GO nanosheets were uniformly dispersed into 160 mg of phosphate-buffered saline (PBS) solution and subjected to ultrasonication for 1 h. Following the ultrasonication, 20 mg of 1-(3-dimethylaminopropyl)-3-ethylcarbodiimide (EDC) and 80 mg of *N*-hydroxysuccinimide (NHS) were added to the dispersion to preactivate the carboxyl and epoxy groups on the GO nanosheets. To this mixture, 20 mg of Arg was introduced, and the solution was stirred overnight at room temperature. The resulting solution was then thoroughly washed and transferred into a dialysis bag, where it was dialyzed for 5–7 days to yield Arg-functionalized GO nanosheets at a concentration of 1 mg mL^{-1}.

2.3. Fabrication of GO, Arg-GO and Arg-rGO membranes

In a centrifuge tube, 3 mL of the pre-prepared Arg-GO dispersion was added and diluted to 50 mL with deionized water, followed by sonication for 10 min to achieve a homogeneous dispersion. The resulting dispersion was then subjected to vacuum filtration, allowing the Arg-GO nanosheets to be uniformly deposited onto a cellulose ester membrane (MCE, 50 mm diameter, 0.22 μm pore size). This membrane was designated as the Arg-GO membrane. Similarly, GO membranes were fabricated using a pre-prepared GO dispersion. Notably, Arg-GO membranes were dried in a vacuum oven at 140 °C for 1 h within the filtration flask to obtain the final Arg-rGO membranes.

2.4. Membrane separation performance tests

Nanofiltration experiments were conducted using a vacuum filtration unit. For the individual ion nanofiltration tests, the feed solution comprised 200 mL of a 300 ppm single salt solution (KCl, LiCl, NaCl, $MgCl_2$, and $CaCl_2$). The filtrate was collected under a pressure of 1 bar, subsequently diluted several times, and analyzed for cation concentrations using inductively coupled plasma optical emission spectroscopy (ICP-OES). In the mixed ion separation tests, the feed solution was replaced with a mixture of lithium chloride and magnesium chloride at different mass ratios. The experimental procedures followed were consistent with those used in the individual ion permeation tests.

Furthermore, a crossflow filtration unit was employed in the separation experiments simulating brines. The system operated at a pressure of 3 bars, with a feed concentration of 2100 ppm (comprising 2000 ppm $MgCl_2$ and 100 ppm LiCl) in the mixed solution.

Finally, water permeance J_s (L m^{-2} h^{-1} bar^{-1}), rejection rate R (%) and the separation factor of Mg^{2+} and Li^{+} ($S_{Li/Mg}$) were measured as follows:

$$J_s = \frac{V}{\Delta t \times A \times P} \quad (1)$$

$$R = \left(1 - \frac{C_p}{C_f}\right) \times 100\% \quad (2)$$

$$S_{\frac{Li}{Mg}} = \frac{C_{Li,p}/C_{Mg,p}}{C_{Li,f}/C_{Mg,f}} \quad (3)$$

where V represents the volume of the filtrate, Δt is the permeance time, A is the effective membrane area of 1.13×10^{-3} m^2, and P is applied pressure. Inductive coupled plasma-optical emission spectrometry (ICP-OES, iCAP 7400, Thermo Fisher Scientific) was employed to measure the ion concentrations of the permeate (C_p) and feed (C_f) solutions.

3. Result and discussion

3.1. Preparation and characterization of thermally reduced Arg-rGO nanofiltration membranes with positive charge

To achieve positively charged rGO membranes with controlled interlayer spacing suitable for the separation of lithium and magnesium ions, we first activated the carboxyl and epoxy groups on the GO surface using EDC and NHS. Subsequently, Arg was grafted onto the GO nanosheets through continuous stirring, resulting in the formation of Arg-GO nanosheets. These grafted nanosheets were then filtered and formed a membrane under a pressure of 0.1 MPa. To precisely control the interlayer spacing, the membrane was subjected to a thermal reduction treatment at 140 °C for 1 h. The resulting membranes, as depicted in Fig. 1(a), were identified as Arg-rGO membranes. The zeta potential of the Arg-GO suspensions was subsequently

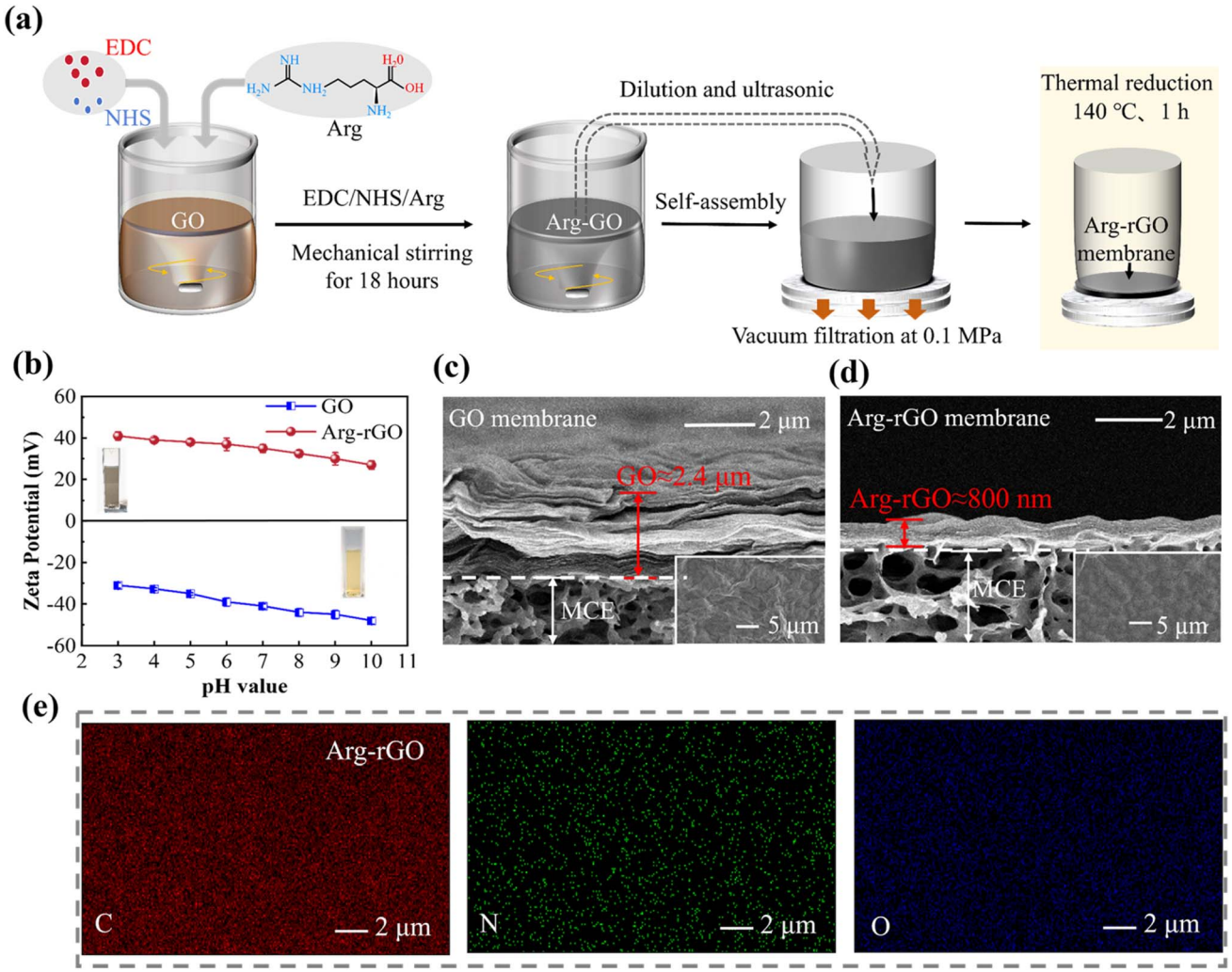

Fig. 1 (a) Schematic of preparation of Arg-rGO nanofiltration membranes. (b) Comparison of zeta potentials of GO and Arg-rGO suspensions at different pH values. (c and d) Surface morphology and cross-sectional images of the GO and Arg-rGO membrane characterized by SEM. (e) EDS mapping of the Arg-rGO membrane containing C, N, and O elements.

measured, as shown in Fig. 1(b), which are positively charged. This is attributed to the presence of guanidino groups in the Arg side chains, which consist of a carbon atom and three positively charged amino groups. The abundant positively charged amino groups partially neutralize the negative charge of the GO nanosheets, with the remaining negative charge exposed to the surrounding environment, resulting in a positively charged surface for the Arg-graphene oxide nanosheets.[38] In contrast, GO suspensions exhibit a negative charge due to the ionization of the oxygen-containing functional groups on the surface of the graphene oxide nanosheets.[39,40] These zeta potential measurements further confirm the successful attachment of Arg amino acid onto the surface of the GO nanosheets. When stacked into membranes, the charged Arg-rGO nanosheets can form positively charged nanochannels.

The surface morphology and cross-sectional images of GO and Arg-rGO membranes were characterized using scanning electron microscopy (SEM). As shown in Fig. 1(c), the GO membrane exhibits a thickness of approximately 2.4 μm and has a two-dimensional layered structure with no significant surface defects. In contrast, the Arg-rGO membrane in Fig. 1(d), displays a smoother surface morphology and an improved fold structure resulting from the Arg modification. Additionally, the smaller thickness of approximately 800 nm of Arg-rGO membrane can be attributable to the removal of a portion of the oxygen-containing functional groups on GO membrane by the thermal reduction treatment. This reduction in membrane thickness indicates that the Arg-rGO membrane has the smaller interlayer spacing, which will enhance both the electrostatic repulsion and size exclusion in the Arg-rGO membrane for efficient separation of lithium and magnesium ions. As illustrated in Fig. 1(d), the laminar structure of the Arg-rGO membrane enables both high separation efficiency and rapid cation transport,[24] while, the porous structure below represents the mixed cellulose ester (MCE) substrate used during the membrane preparation process. The elemental mapping of the Arg-rGO membrane is presented in Fig. 1(e). The nitrogen (N) content in the Arg-rGO membrane is notably higher compared

to the GO membrane (Fig. S1†), and its distribution is uniform and continuous throughout the region. These findings further confirm the successful crosslinking of Arg onto the GO nanosheets. TGA analysis was performed on the samples before and after arginine grafting (Fig. S2†). Compared to the GO membrane, the Arg-rGO membrane exhibits a significant mass loss around 245 °C,[41] which corresponds to the thermal decomposition temperature of arginine. This further confirms the successful grafting of arginine onto the GO surface.

X-ray photoelectron spectroscopy (XPS) was employed to further analyze the element and functional group changes of these membranes. Compared with the XPS spectrum of the GO membrane, the XPS spectrum of Arg-rGO membrane shows a distinct peak at 399.8 eV corresponding to the nitrogen (N) element (Fig. 2(a)). The N 1s spectrum of Arg-rGO membrane can be deconvoluted into two peaks corresponding to C–NH_2 and C–NH_3^+ components (Fig. 2(b)), representing the amine group (91.14%) and protonated guanidinium group (8.86%) in arginine, respectively and further suggesting the successful incorporation of Arg onto the membranes.[42] The XPS C 1s spectrum of the Arg-rGO membrane (Fig. 2(c)), could be fitted to three peaks, with binding energies at 284.4, 286.4, and 287.8 eV, corresponding to C–C, C–O/C–N, and C═O bonds, respectively.[43] The relative percentages of these components were found to be 7.38%, 36.02%, and 56.60%, respectively. Specifically, the amino group of Arg reacts with the C–O groups on the GO nanosheets, leading to the formation of C–N covalent bonds. But, no distinct C–N bond is observed because it is overshadowed by the C–O bond. Additionally, compared to the GO membrane (Fig. S3(a)†), the total intensities at C–O/C–N position of both the Arg-GO (Fig. S3(b)†) and the Arg-rGO (Fig. 2(c)) membrane reduced, due to the thermal decomposition of hydroxyl in the GO structure during thermal treatment. This reduction in oxygen content not only decreases the interlayer spacing of the membrane, resulting in a more ordered structure, but also stabilizes the amino groups between the layers. Additionally, the C–C bond, which represents the sp^2 hybridized carbon atoms on the GO surface, is also present, with its content reflecting the covalent bonding of some carbon atoms with Arg. The C 1s spectrum of the Arg-rGO membrane (Fig. 2(c)) exhibited peak species identical to those observed in the Arg-GO membrane (Fig. S3(b)†); however, the content of C–C bonds increased from 47.36% to 56.60%. This increase is attributed to the thermal treatment, which promotes the conversion of sp^3 carbon to sp^2 carbon, facilitating the re-formation of π-bonds between carbon atoms. The O 1s spectra (Fig. S4†) were deconvoluted into four components: C═O (531.4 eV), C–O–C (532.2 eV), C–OH (533.8 eV), and –COOH (533.3 eV). The decrease in intensity of the C–OH peak after grafting is consistent with that after the thermal reduction, whereas the increase in intensity of the peak at 531.4 eV is attributed to the formation of amide bonds from the reaction.[44]

The interlayer spacing changes in the GO, Arg-GO, and Arg-rGO membranes were investigated through X-ray diffraction (XRD) characterization (Fig. 3(a)). The characteristic peak of the (001) crystal plane of GO is located at $2\theta = 12.5°$, with an interlayer spacing of approximately 7.2 Å, showing a sharp and high-intensity peak, indicating the ordered stacking structure of the GO sheets. The XRD peak of the Arg-GO membrane shifts to a lower angle, corresponding to an increased interlayer spacing of 8.1 Å, due to the arginine molecules grafted onto the GO sheets *via* covalent bonds. While, the interlayer spacing of the Arg-rGO membrane has a little decrease to 7.9 Å compared with the Arg-GO membrane, resulting from the removal of some hydroxyl groups by thermal treatment which will reduce the hydrophilicity, steric effect, and electrostatic repulsion of GO sheets. Notably, the final effective size of the Arg-rGO nanochannels is closely aligned with the hydrated ionic diameter of Li^+, while being significantly smaller than that of Mg^{2+}. Furthermore, electrostatic interactions and crosslinking between the Arg molecules and the GO nanosheets effectively prevented swelling between the nanosheets. This fixed interlayer spacing in aqueous solutions not only enhances the membrane's structural stability but also contributes to its efficiency in ion separation.

The contact angles of the GO, Arg-GO, and Arg-rGO membranes were also measured. As in Fig. 3(b) showing, the GO membrane displays a degree of hydrophilicity, as evidenced by its contact angle of 44°, reflecting its high content of oxygen-containing functional groups on the surface. While, the contact

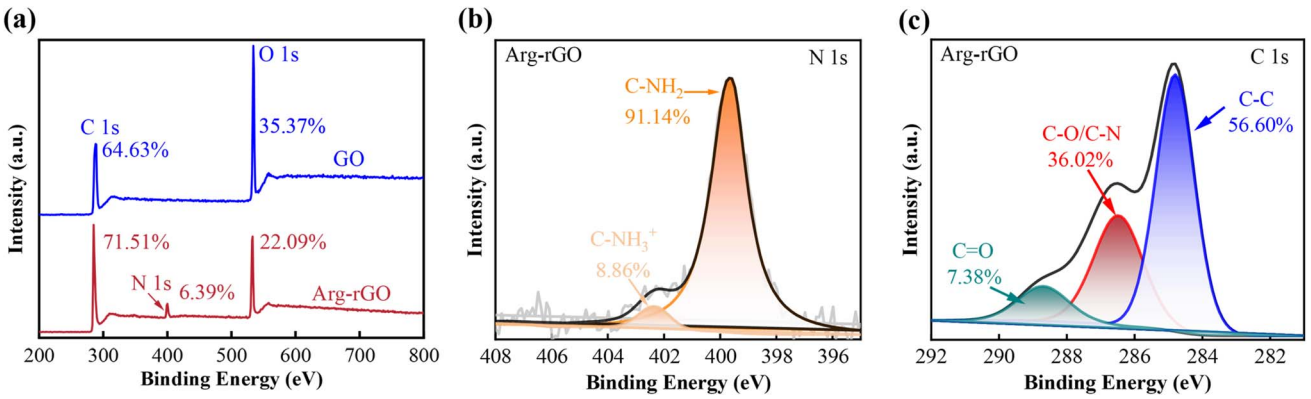

Fig. 2 (a) X-ray photoelectron spectroscopy (XPS) survey spectra of the GO and Arg-rGO membranes. (b) N 1s spectrum of Arg-rGO membrane. (c) C 1s spectrum of Arg-rGO membrane.

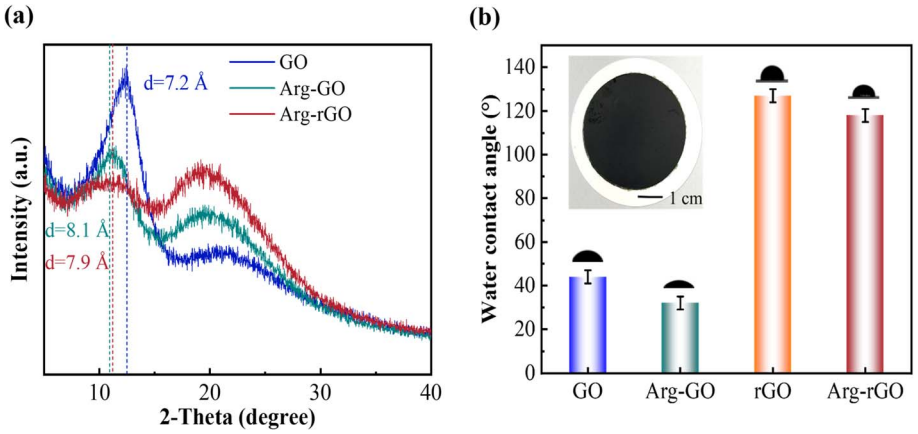

Fig. 3 (a) X-ray diffraction (XRD) spectra of the GO, Arg-GO, and Arg-rGO membranes. (b) Contact angle (CA) of the GO, Arg-GO, rGO and Arg-rGO membranes. Inset is a digital photograph of membrane.

angle of the Arg-GO membrane decreased to 32°, resulting from the grafted Arg molecules, which increased the presence of additional functional groups, such as the amino groups (*e.g.*, $-NH_2$) and oxygen-containing groups (*e.g.*, –COOH, –OH). After thermal reduction treatment, the contact angle of the rGO and Arg-rGO membranes rose to 127° and 118°, respectively, which can be attributed to the removal of a significant amount of oxygen-containing functional groups. And the enhanced hydrophobicity facilitates the ion transport within the nanochannels in the aqueous state, leading to the water permeance improvement of the Arg-rGO membrane for magnesium-lithium separation.

3.2. Nanofiltration behavior of GO and Arg-rGO membranes for various salt ions

As shown in Fig. 4(a), the GO membranes exhibited relatively low rejection (approximately 40%) for monovalent cations, such as K^+, Na^+, and Li^+. In contrast, the rejection rates for divalent cations, Ca^{2+} and Mg^{2+}, were relatively higher, at approximately 78.2% and 82.4%, respectively. In contrast, the Arg-rGO membranes exhibited an enhanced rejection of monovalent cations, such as K^+, Na^+, and Li^+, reaching around 50%. Remarkably, the rejection rates for divalent cations, Ca^{2+} and Mg^{2+}, were significantly increased to 96.9% and 98.2%, respectively. The water permeances of Arg-rGO membranes are relatively low compared to GO membranes (Fig. 4(b)). This substantial improvement in rejection can be attributed to both the Donnan effect[38] and size exclusion mechanisms.[41] The positively charged Arg residues on the surface of the Arg-rGO membrane create electrostatic repulsion, particularly for divalent cations with higher valence states. Furthermore, the size of the nanochannels in the Arg-rGO membrane, which is between the hydration diameters of lithium and magnesium ions, coupled with the hydrophobicity of this membrane, will promisingly contribute to the improvement in separation performance.

3.3. Separation performance of Arg-rGO membranes for magnesium and lithium

The impact of salt concentration on the performance of Arg-rGO membranes was investigated. As the concentration of the mixed solution of $MgCl_2$ and LiCl (with Mg^{2+}/Li^+ mass ratio of 20 : 1) was increased from 50 to 500 ppm, the water permeance decreased significantly from 52 to 12 L m^{-2} h^{-1} bar^{-1}. This reduction can be attributed to the osmotic pressure generated by the solutes on both sides of the membrane, which counteracts a portion of the applied driving pressure, in addition to the concentration polarization occurring at the membrane surface.

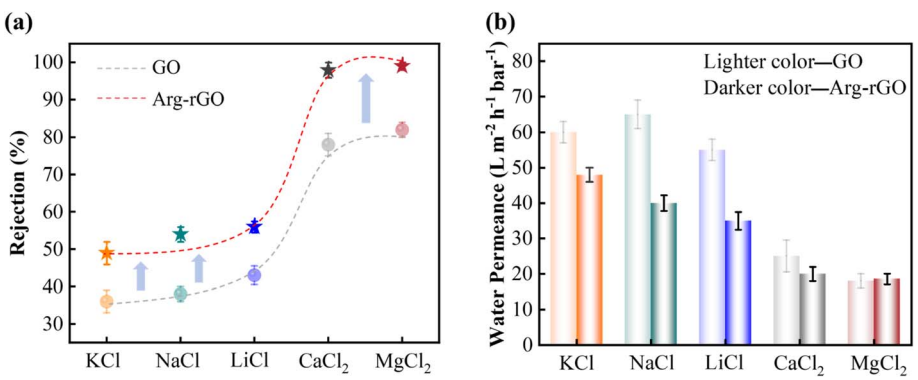

Fig. 4 (a) Rejection of Arg-rGO and GO membranes for salt ions at a feed concentration of 300 ppm (KCl, NaCl, LiCl, $CaCl_2$, and $MgCl_2$). (b) Water permeance of Arg-rGO and GO membranes.

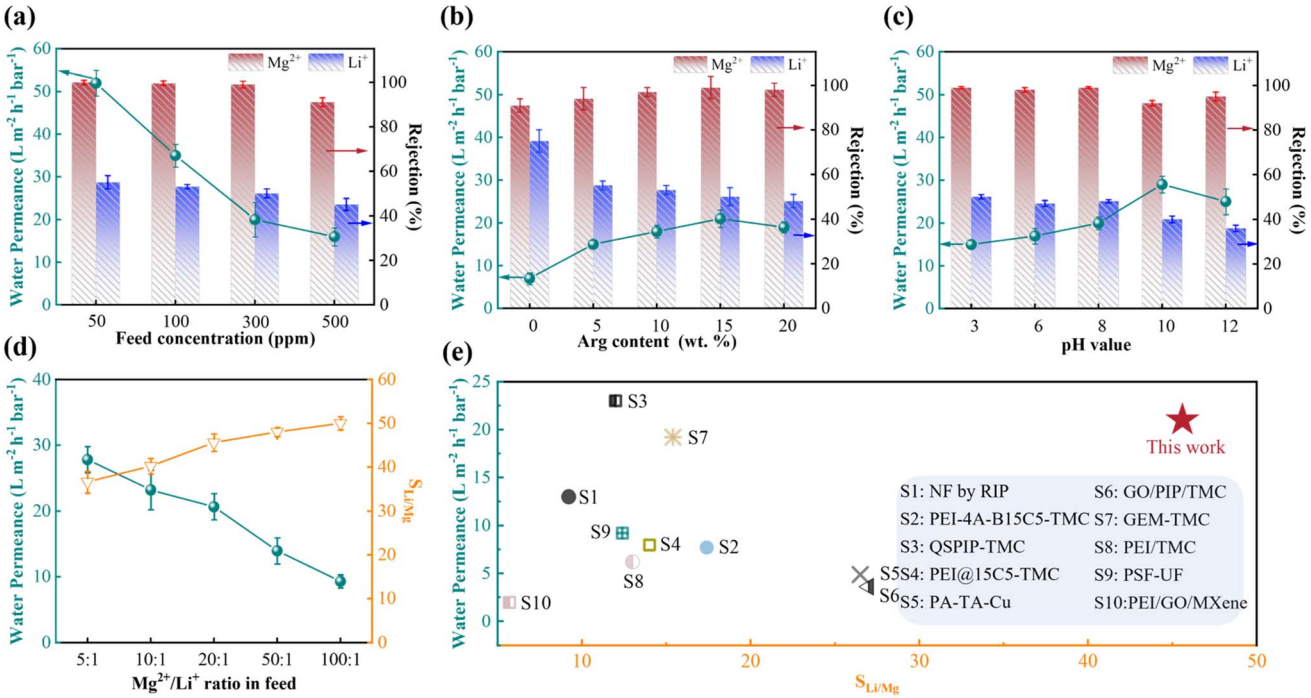

Fig. 5 (a–c) Water permeances and rejection rates of Arg-rGO membranes for magnesium–lithium mixed solutions under varying conditions including different feed solution concentrations, percentages of Arg addition, and pH values. (d) $S_{Li/Mg}$ of Arg-rGO membrane for different Mg^{2+}/Li^+ ratios. (e) Comparison of $S_{Li/Mg}$ and water permeance of the reported membranes.

Despite this permeance decline, the rejection of $MgCl_2$ remained above 91% (Fig. 5(a)), whereas the rejection of LiCl decreased from 55.2% to 45.7% as the LiCl concentration in the feed solution increased. We investigated the separation performance of Arg-rGO membranes on lithium–magnesium mixed solutions at different reduction temperatures and determined 120 °C as the optimal reduction temperature (Fig. S5†).

Fig. 5(b) illustrates the influence of different amounts of Arg loadings on the separation performance of the Arg-rGO membranes. As the percentage of Arg addition increased from 5% to 20%, the rejection of the Arg-rGO membrane to Mg^{2+} increased from 91% to stabilize at 98.2%, while the rejection rate to Li^+ decreased from an initial value of 75% to approximately 50%. The efficient rejection of Mg^{2+} was primarily attributed to the electrostatic repulsion exerted by the positive charges within the nanochannels, which effectively repelled ions with higher valence states. Conversely, the reduction in Li^+ rejection was associated with the increase and stabilization of the nanochannel dimensions in rGO due to the membrane functionalization by Arg insertion. These results demonstrate that the most significant difference in the rejection rates of Li^+ and Mg^{2+}, along with the optimal separation performance, was achieved with an Arg addition of 15%.

Subsequently, we investigated the effect of Arg-rGO membranes on Mg^{2+}/Li^+ separation across a wide pH range of 3–12, as presented in Fig. 5(c). As the pH increased, the permeance of the Arg-rGO membrane gradually rose, while the rejection rate for Mg^{2+} remained consistently above 98.2%, primarily due to charge repulsion. However, when the pH exceeded 10, the permeance and the rejection rate for Mg^{2+} were decreased. These observations correlate with the zeta potential data shown in Fig. 1(b) and align with findings reported in previous studies.[45] Arg, being an amphiphilic molecule, exhibits a pH-dependent charge behavior. When the pH is below 10.76 (the isoelectric point of Arg), the molecule carries a positive charge, rendering the nanochannels positively charged as well. This facilitates electrostatic repulsion against cations, such as Mg^{2+}. In contrast, when the pH surpasses 10.76, Arg becomes negatively charged, causing the nanochannels to acquire an overall negative charge. As a result, the electrostatic repulsion towards cations is diminished, which likely contributes to the reduced rejection of $MgCl_2$. Noteworthy, the observed $MgCl_2$ repulsion at a high pH value around 12, may be due to size exclusion and the $Mg(OH)_2$ formation.[45]

Furthermore, in order to respectively investigate the effects of electrostatic repulsion and size exclusion on Mg^{2+}/Li^+ separation performance of the Arg-rGO membrane, the separation factors of four types of membranes—the GO, rGO, Arg-GO, and Arg-rGO membranes were obtained under the same experimental conditions. As shown in Fig. S6,† the separation factors for these membranes were 2.3, 9.8, 16.2, and 45.6, respectively. The rejections of the GO membrane for Li^+ and Mg^{2+} are 43% and 82%, respectively. In comparison with the GO membrane, the rejections of Li^+ and Mg^{2+} by the partially reduced rGO membrane has been improved to 50% and 94%, and the separation factors increased from 2.3 to 9.8, which can be attributed to the enhancement of the size exclusion within the rGO membrane with smaller interlayer spacing (Fig. 3(a)). For the Arg-GO membrane, the rejections of Li^+ and Mg^{2+} were 45% and 93%,

respectively, and the separation factors increased from 2.3 to 16.9 compared with the GO membrane. The result obtained here can be ascribed to the Arg amino acid modification, which serves to augment the electrostatic repulsion effect of the membrane, particularly in the context of divalent Mg^{2+} ions. Furthermore, within the Arg-rGO membrane, benefitting from the synergistic effect of electrostatic repulsion and size exclusion led to a substantial improvement in the separation factor, the separation factors of the Arg-rGO membrane sharply increased from 2.3 to 45.6 compared with the GO membrane, and the rejections of Li^+ and Mg^{2+} were also increased to 56% and 99%, respectively.

The impacts of the Mg^{2+}/Li^+ ratio in the feed mixture on the separation performance of the Arg-rGO membrane were monitored. In Fig. 5(d), as the Mg^{2+}/Li^+ ratio increased from 5 : 1 to 100 : 1, the water permeance gradually decreased to 9.3 L m^{-2} h^{-1} bar^{-1}, while the $S_{Li/Mg}$ steadily increased to 51. For comparison, we selected the usual Mg^{2+}/Li^+ ratio of 20 : 1 and benchmarked it against reported nanofiltration membranes. The results demonstrated that Arg-rGO membranes exhibit a distinct advantage, with higher $S_{Li/Mg}$ at an elevated water permeance, as shown in Fig. 5(e) and Table S1 of the ESI.†

3.4. Two-stage crossflow filtration to separate simulated salt lakes brine

The practical application potential of the Arg-rGO membrane was tested on a simulated brine with a Mg^{2+}/Li^+ mass ratio of 20.[35] As shown in Fig. 6(a), a two-stage crossflow filtration was employed to purity the brine with a Mg^{2+}/Li^+ mass ratio of 20. The brine was first subjected to crossflow filtration at 3 bars (Fig. 6(b)), showing that the initial Mg^{2+}/Li^+ mass ratio in the feed was 20, which significantly decreased to 6.4 after the first treatment stage. Following the 2nd stage nanofiltration (NF), the Mg^{2+}/Li^+ ratio further decreased to 0.2, demonstrating the high efficiency of the process in removing magnesium ions from the simulated brine. The water flux during the 1st stage was 42.6 L m^{-2} h^{-1} (Fig. 6(c)), which was lower primarily due to the high concentration of the feed solution and the resulting elevated osmotic pressure on both sides of the membrane, which reduced the effective driving pressure. In contrast, the water flux in the 2nd stage increased to 75.3 L m^{-2} h^{-1}, superior to the reported performance. Therefore, the Arg-rGO membranes demonstrated both high selectivity and exceptional permeance for Mg^{2+}/Li^+ separation.

3.5. Long-term and mechanical stability tests

To validate the practical application potential of the membrane, the long-term stability of the Arg-rGO membrane was evaluated by a cross-flow filtration experiment (the setup is shown in Fig. S7†). The result as shown in Fig. 7(a), the Arg-rGO membrane maintained a high rejection rate for Mg^{2+} (>90%) and a selective permeation for Li^+ (<45%) within a 60 hour operation. Furthermore, both the GO and rGO membranes were structurally damaged and lost their original integrity within 10 s of ultrasonication (360 kW). In contrast, the Arg-rGO membrane retained its original integrity within 600 s of ultrasonication (360 kW), demonstrating the excellent mechanical stability of

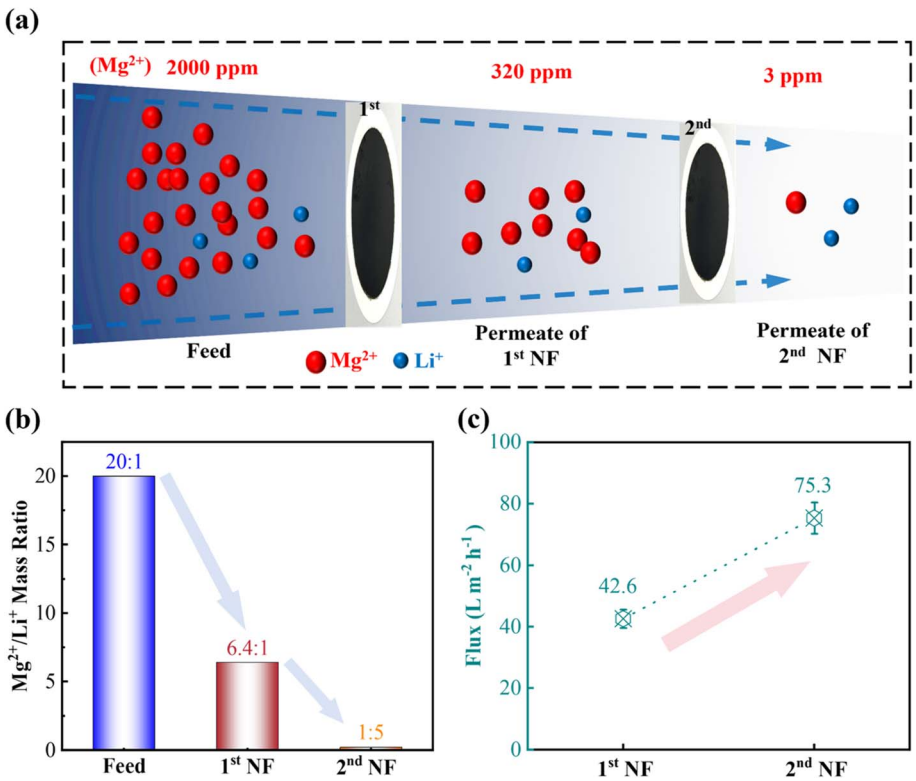

Fig. 6 (a) A schematic of the two-stage crossflow filtration for concentrated salt mixtures at a pressure of 3 bars (2000 ppm Mg^{2+}, 100 ppm Li^+). (b and c) Mg^{2+}/Li^+ ratio and water flux after the first and second crossflow nanofiltration stages using the Arg-rGO membrane.

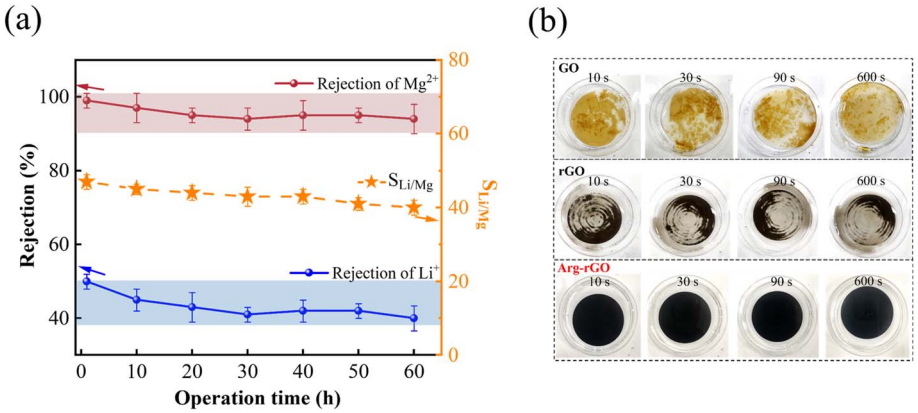

Fig. 7 (a) Long-term stability of the Arg-rGO membrane. (b) Comparison of the mechanical stability of the GO, rGO, and Arg-rGO membranes.

the Arg-rGO membrane (Fig. 7(b)). These results confirm the superior stability and durability of the Arg-rGO membrane, thereby enhancing the practical applicability of our findings.

4. Conclusions

In conclusion, a positively charged nanochannel membrane was constructed by functionally modified Arg amino acid grafted onto GO nanosheets and the interlayer spacing of the membrane was further regulated by thermal reduction. For Mg^{2+}/Li^+ mixtures with a typical mass ratio of 20, the $S_{Li/Mg}$ were enhanced to 45.6, with a high water permeance of 21.3 L m^{-2} h^{-1} bar^{-1}. Additionally, after two-stage crossflow filtration, the Mg^{2+}/Li^+ ratio can be reduced from 20 to 0.2.

These findings on charge modification and interlayer spacing control of GO-based membranes have led to the efficient separation of Mg^{2+}/Li^+. This demonstrates a sustainable and cost-effective method using GO-based membranes for practical application in lithium extraction from salt lakes. Furthermore, this technology not only offers a promising solution for lithium recovery but also has the potential to be adapted for the separation of other valuable ions from saline environments.

Data availability

Data will be made available on request.

Author contributions

Pei Li and Liang Chen: conceptualization, funding acquisition, supervision and writing – review & editing; Junbo Wang: date curation, investigation, methodology, validation, supervision and writing – original draft; Jie Jiang: methodology, supervision and visualization. All authors discussed the results and commented on the manuscript.

Conflicts of interest

The authors declare that they have no known competing financial interests or personal relationships that could have appeared to influence the work reported in this paper.

Acknowledgements

Junbo Wang and Jie Jiang contributed equally to this work. The authors were supported by the National Natural Science Foundation of China (No. 12074341), the Scientific Research and Developed Funds of Ningbo University (No. ZX2022000015), Public Welfare Research Project of Ningbo (No. 2024S066) and State Key Laboratory of Surface Physics and Department of Physics, Fudan University, Shanghai 200433, P. R. China (No. KF2023_07).

References

1 J. T. Frith, M. J. Lacey and U. Ulissi, A non-academic perspective on the future of lithium-based batteries, *Nat. Commun.*, 2023, **14**, 420.
2 T. Wulandari, D. Fawcett, S. B. Majumder and G. E. J. Poinern, Lithium-based batteries, history, current status, challenges, and future perspectives, *Battery Energy*, 2023, **2**, 20230030.
3 H. Geng, Y. Peng, L. Qu, H. Zhang and M. Wu, Structure Design and Composition Engineering of Carbon-Based Nanomaterials for Lithium Energy Storage, *Adv. Energy Mater.*, 2020, **10**, 1903030.
4 S. Yang, Y. Wang, H. Pan, P. He and H. Zhou, Lithium extraction from low-quality brines, *Nature*, 2024, **636**, 309–321.
5 O. A. Kazi, W. Chen, J. G. Eatman, F. Gao, Y. Liu, Y. Wang, Z. Xia and S. B. Darling, *Adv. Mater.*, 2023, **35**, 2300913.
6 M. Yong, M. Tang, L. Sun, F. Xiong, L. Xie, G. Zeng, X. Ren, K. Wang, Y. Cheng, Z. Li, E. Li, X. Zhang and H. Wang, Sustainable lithium extraction and magnesium hydroxide co-production from salt-lake brines, *Nat. Sustain.*, 2024, **7**, 1662–1671.
7 Y. Sun, Q. Wang, Y. Wang, R. Yun and X. Xiang, Recent advances in magnesium/lithium separation and lithium extraction technologies from salt lake brine, *Sep. Purif. Technol.*, 2021, **256**, 117807.
8 M. L. Vera, W. R. Torres, C. I. Galli, A. Chagnes and V. Flexer, Environmental impact of direct lithium extraction from brines, *Nat. Rev. Earth Environ.*, 2023, **4**, 149–165.

9 Y. Jiang, G. Zhang, K. Zhou, C. Peng, K. A. M. Salih, H. Zhou, Y. Wu and W. Chen, Sequential separation and recovery of phosphorus and lithium from lithium phosphate slag by selective extraction–precipitation, *Sep. Purif. Technol.*, 2024, **333**, 125907.
10 Y. Song and Z. Zhao, Recovery of lithium from spent lithium-ion batteries using precipitation and electrodialysis techniques, *Sep. Purif. Technol.*, 2018, **206**, 335–342.
11 G. Liu, Z. Zhao and A. Ghahreman, Novel approaches for lithium extraction from salt-lake brines: a review, *Hydrometallurgy*, 2019, **187**, 81–100.
12 S. Wang, S. Zheng, Z. Wang, W. Cui, H. Zhang, L. Yang, Y. Zhang and P. Li, Superior lithium adsorption and required magnetic separation behavior of iron-doped lithium ion-sieves, *Chem. Eng. J.*, 2018, **332**, 160–168.
13 S. Wang, X. Chen, Y. Zhang, Y. Zhang and S. Zheng, Lithium adsorption from brine by iron-doped titanium lithium ion sieves, *Particuology*, 2018, **41**, 40–47.
14 F. Degen, M. Winter, D. Bendig and J. Tübke, Energy consumption of current and future production of lithium-ion and post lithium-ion battery cells, *Nat. Energy*, 2023, **8**, 1284–1295.
15 J. Li, L. Li, R. Yang and J. Jiao, Assessment of the lifecycle carbon emission and energy consumption of lithium-ion power batteries recycling: a systematic review and meta-analysis, *J. Energy Storage*, 2023, **65**, 107306.
16 J. Xu, X. Cai, S. Cai, Y. Shao, C. Hu, S. Lu and S. Ding, High-Energy Lithium-Ion Batteries: Recent Progress and a Promising Future in Applications, *Energy Environ. Mater.*, 2023, **6**, 12450.
17 R. Xu, Y. Kang, W. Zhang, B. Pan and X. Zhang, Two-dimensional MXene membranes with biomimetic sub-nanochannels for enhanced cation sieving, *Nat. Commun.*, 2023, **14**, 4907.
18 M. I. Walker, K. Ubych, V. Saraswat, E. A. Chalklen, P. Braeuninger-Weimer, S. Caneva, R. S. Weatherup, S. Hofmann and U. F. Keyser, Extrinsic Cation Selectivity of 2D Membranes, *ACS Nano*, 2017, **11**, 1340–1346.
19 S. Kim, H. Choi, B. Kim, G. Lim, T. Kim, M. Lee, H. Ra, J. Yeom, M. Kim, E. Kim, J. Hwang, J. S. Lee and W. Shim, Extreme Ion-Transport Inorganic 2D Membranes for Nanofluidic Applications, *Adv. Mater.*, 2023, **35**, 2206354.
20 G. Zhao, Y. Zhang, Y. Li, G. Pan and Y. Liu, *Adv. Membr.*, 2023, **3**, 100065.
21 J. Hou, H. Zhang, A. W. Thornton, A. J. Hill, H. Wang and K. Konstas, Lithium Extraction by Emerging Metal–Organic Framework-Based Membranes, *Adv. Funct. Mater.*, 2021, **31**, 2105991.
22 H. M. Saif, J. G. Crespo and S. Pawlowski, Lithium recovery from brines by lithium membrane flow capacitive deionization (Li-MFCDI) – a proof of concept, *J. Membr. Sci.*, 2023, **3**, 100059.
23 B. Mi, Graphene Oxide Membranes for Ionic and Molecular Sieving, *Science*, 2014, **343**, 740–742.
24 I. Chandio, F. A. Janjhi, A. A. Memon, S. Memon, Z. Ali, K. H. Thebo, A. A. A. Pirzado, A. A. Hakro and W. S. Khan, Ultrafast ionic and molecular sieving through graphene oxide based composite membranes, *Desalination*, 2021, **500**, 114848.
25 P. Sun, M. Zhu, K. Wang, M. Zhong, J. Wei, D. Wu, Z. Xu and H. Zhu, Selective Ion Penetration of Graphene Oxide Membranes, *ACS Nano*, 2013, **7**, 428–437.
26 F. Soomro, A. Ali, S. Ullah, M. Iqbal, T. Alshahrani, F. Khan, J. Yang and K. H. Thebo, *Langmuir*, 2023, **39**, 18447–18457.
27 L. Xie, J. Tang, R. Qin, Q. Zhang, J. Liu, Y. Jin and H. Wang, Surface Charge Modification on 2D Nanofluidic Membrane for Regulating Ion Transport, *Adv. Funct. Mater.*, 2023, **33**, 2208959.
28 M. Zhang, K. Guan, Y. Ji, G. Liu, W. Jin and N. Xu, Controllable ion transport by surface-charged graphene oxide membrane, *Nat. Commun.*, 2019, **10**, 1253.
29 J. Fu, M. Zhang, L. Jin, L. Liu, N. Li, L. Shang, M. Li, L. Xiao and Y. Ao, Enhancing interfacial properties of carbon fibers reinforced epoxy composites *via* Layer-by-Layer self assembly GO/SiO_2 multilayers membranes on carbon fibers surface, *Appl. Surf. Sci.*, 2019, **470**, 543–554.
30 J. Zhang, X. Li, F. Yang, Z. Ouyang, P. He, Z. Jia, H. Long, N. He, Y. Zhang, Y. Zou, B. Jiang, Z. Han, G. Tao, N. Liu, Y. Li and L. Ma, Interlaced Composite Membranes by Charge-Induced Alternating Assembly of Monolayer Cationic COF and GO, *ACS Appl. Mater. Interfaces*, 2024, **16**, 68306–68315.
31 A. Avornyo and C. V. Chrysikopoulos, Applications of graphene oxide (GO) in oily wastewater treatment: recent developments, challenges, and opportunities, *ACS Appl. Mater. Interfaces*, 2024, **353**, 120178.
32 H. Jafarian, M. Dadashi Firouzjaei, S. Aghapour Aktij, A. Aghaei, M. Pilevar Khomami, M. Elliott, E. K. Wujcik, M. Sadrzadeh and A. Rahimpour, Synthesis of heterogeneous metal organic framework-graphene oxide nanocomposite membranes for water treatment, *Chem. Eng. J.*, 2023, **455**, 140851.
33 R. Li, D. Guan, M. Wen, X. Zhang, M. Chen, H. Yang and C. Xu, Tuning interlayer spacing of graphene oxide membrane to enhance its separation performance of hydrogen isotopic water in membrane distillation, *Sep. Purif. Technol.*, 2023, **304**, 122382.
34 C. Mao, H. Shao, C. Huang, L. Chen, L. Ma, Y. Ren, M. Tu, H. Wang, J. Gu, H. Ma and G. Xu, Revealing the role of interlayer spacing in radioactive-ion sieving of functionalized graphene membranes, *J. Hazard. Mater.*, 2024, **475**, 134795.
35 S. Wei, X. Ding, Y. Qiu, V. De Waele and H. Guo, Enhanced performance polyamide membrane by introducing high-porosity SOD/GO composite interlayer to tailor the interfacial polymerization process, *Chem. Eng. J.*, 2024, **481**, 148595.
36 R. Krishnamoorthi, F. S. Butt, N. A. Mazlan, S. Chen, N. Radacsi, S. Yang, Y. Yoon and Y. Huang, Tuning the interlayer spacing of graphene oxide membrane *via* surfactant intercalation for ultrafast nanofiltration, *J. Membr. Sci.*, 2024, **706**, 122942.
37 J. Wang, A. Wang, J. Liu, Q. Niu, Y. Zhang, P. Liu, C. Liu, H. Wang, X. Zeng and G. Zeng, Polyethyleneimine

Modified Two-Dimensional GO/MXene Composite Membranes with Enhanced Mg^{2+}/Li^{+} Separation Performance for Salt Lake Brine, *Molecules*, 2024, **29**, 184326.

38 M. Li, C. Liu, Y. Xie, H. Cao, H. Zhao and Y. Zhang, The evolution of surface charge on graphene oxide during the reduction and its application in electroanalysis, *Carbon*, 2014, **66**, 302–311.

39 X. Sun, C. Yang, W. Liu, K. Lu and H. Yin, Charge modifications of graphene oxide enhance the inhibitory effect on insulin amyloid fibrillation based on electrostatic interactions, *Int. J. Biol. Macromol.*, 2023, **225**, 1140–1151.

40 H. Muhtar and A. Darmawan, Fabrication of negatively charged nanofiltration membrane of modified polystyrene intercalated graphene oxide for pervaporation desalination, *Chem. Eng. J.*, 2023, **475**, 146095.

41 I. M. Weiss, C. Muth, R. Drumm and H. O. K. Kirchner, *BMC Biophys.*, 2018, **11**, 2.

42 J. S. Stevens, A. C. de Luca, M. Pelendritis, G. Terenghi, S. Downes and S. L. M. Schroeder, *Surf. Interface Anal.*, 2013, **45**, 1238–1246.

43 O. Jankovský, P. Šimek, K. Klimová, D. Sedmidubský, S. Matějková, M. Pumera and Z. Sofer, *Nanoscale*, 2014, **6**, 6065–6074.

44 N. Alzate-Carvajal, E. V. Basiuk, V. Meza-Laguna, I. Puente-Lee, M. H. Farías, N. Bogdanchikova and V. A. Basiuk, *RSC Adv.*, 2016, **6**, 113596–113610.

45 V. A. Phillips, J. L. Kolbe and H. Opperhauser, Effect of pH on the growth of $Mg(OH)_2$ crystals in an aqueous environment at 60 °C, *J. Cryst. Growth*, 1977, **41**, 228–234.